PCCP

Accepted Manuscript

ROYAL SOCIETY OF CHEMISTRY

www.rsc.org/pccp

Interactions Between Nodes in a Physical Gel Network of Telechelic Polymers; Self-consistent Field Calculations Beyond the Cell Model.

J. Bergsma, F.A.M. Leermakers, J. van der Gucht

Laboratory of Physical Chemistry and Colloid Science, Wageningen University, Dreijenplein 6, 6703 HB, Wageningen, The Netherlands

Abstract

Triblock copolymers, with associative end-groups and a soluble middle block, form flower-like micelles in dilute solutions and a physical gel at higher concentrations. In a gel the middle blocks form bridges between domains/nodes that contain the ends. We combine the self-consistent field theory with a simple molecular model to evaluate the pair potential between the nodes. In this model the end-groups are forced to remain in nodes and the soluble middle blocks are in solution. When the distance between the centres of the nodes is approximately the corona diameter, loops can transform into bridges, and the pair potential is attractive. Due to steric hindrance, the interaction is repulsive at smaller distances.Till now a cell-model has been used wherein a central node interacts through reflecting boundary conditions with its images in a spherical geometry. This artificial approach to estimate pair potentials is here complemented by more realistic three-gradient SCF models. We consider the pair interactions for (i) two isolated nodes, (ii) nodes positioned on a line (iii) a central node surrounded by its neighbours in simple cubic ordering, and (iv) a central node in a face centred cubic configuration of its neighbours. Qualitatively, the cell model is in line with the more refined models, but quantitative differences are significant. We also notice qualitative differences for the pair potentials in the specified geometries, which we interpret as a breakdown of the

pairwise additivity of the pair potential. This implies that for course grained Monte Carlo or molecular dynamics simulations the best choice for the pair potentials depends on the expected node density.

Introduction

Triblock copolymers, with associative end-groups and a soluble middle block, are often referred to as telechelic polymers as they can connect to two different parts. The end-groups can, for example, associate by solvophobic interactions[1,2], charge interactions[3,4] or complexation with metal ions.[5]. These ends form the cores of what may be called micelles. The solvophilic polymeric middle blocks form the corona of these micelles.[6] The steric hindrance between the chains in the corona prevents macroscopic aggregation, and micelles with a limited number of polymers are formed.[7] By mixing the telechelic polymers with a co-surfactant, hybrid micelles can be formed and the average number of polymers per micelle can be adjusted.[8,9] In dilute solutions both ends of the polymers have to be in the same core and a loop is thus formed by the polymer. Because these structures look somewhat like a flower, with the polymer loops as the petals and the micellar core as the heart, they are called flower-like micelles.

When the concentration is increased, the distance between the micelles is reduced and the coronas start to overlap. A loop can then transform into a bridge, thereby connecting two micelles.[2] Of course this can only happen when the anchor energy of the ends is sufficiently low to be overcome by the thermal energy. The possibility to form bridges increases the number of polymer conformations and thus the conformational entropy. This creates an attractive force.[7] When the average number of bridges per micelle is larger than unity, a volume spanning network can be formed.[1] The solution then becomes a gel. Such behaviour is found for the telechelic polymer systems mentioned above. Generically the regions in which the chain ends associate may be referred to as nodes. Similar to chemically crosslinked gels, such associative networks respond elastically upon deformation, but flow at larger time scales.[8] A schematic representation of this gel is shown in figure 1a. In such gel it is the osmotic pressure in the coronal region, i.e. the steric hindrance between solvated corona chains, that keeps the nodes apart. When the number of bridges per node is sufficiently high, the bridging attraction becomes

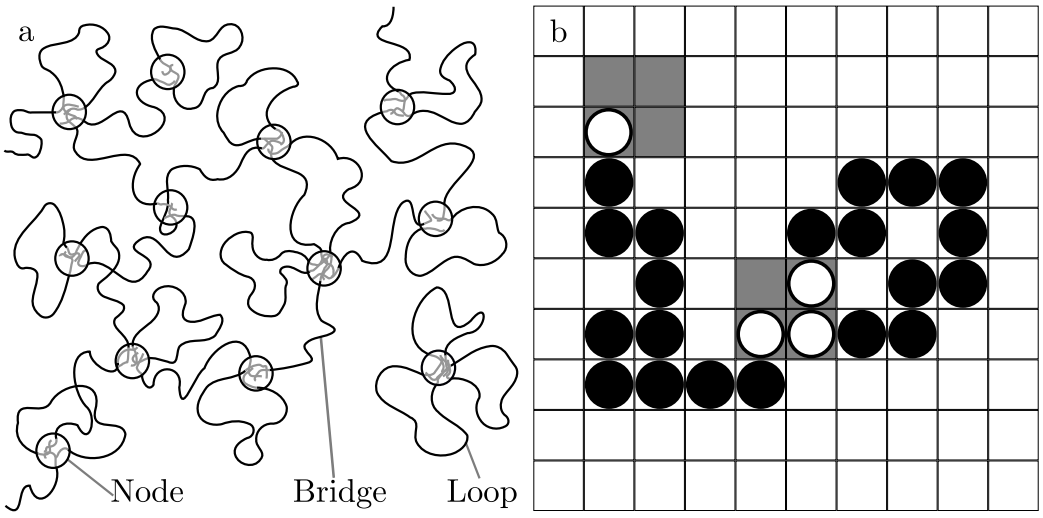

Fig. 1: a: A micellar network formed by telechelic polymers. The circles are the micellar core, with the grey lines as the associative end-groups and the black line as the soluble middle block. The telechelics can form loops (both ends in the same micelle/node) or bridges (ends are in different micelles/nodes). An isolated flower-like micelle is shown in the lower right corner. b: Two polymer configurations, a loop and a bridge (closed circles), on the simple cubic grid with its ends (open circles) constrained within nodes of 2 by 2 lattice sites (grey).

so strong that phase separation occurs.[8] In this case the polymer gel coexists with an excess solvent phase with a relatively low polymer concentration.

Gels made of these telechelics have a wide range of applications. They are, for example, used to improve the rheological properties of paints, as a gel material for gel electrophoresis[10] and are envisioned as carrier material for slow drug release.[11] As the binding of the end-groups is reversible the gels have the property to heal themselves when they are damaged.[12,13]

As already elaborated above, there have been many experimental studies on these systems. The number of theoretical counterparts is, however, limited, basically because the system poses significant theoretical challenges. One way to gain additional insights in the physical properties of such systems is to use computer simulations.

As it is virtually impossible to take all degrees of freedom of the poly-

mers explicitly into account, it is necessary to use a so-called coarse grained model. For example by coarse graining the polymer as a chain of beads, or by modelling a micellar object as a single particle with appropriate pairwise additive interactions between them.[14] To implement the latter method, one needs to determine the free energy of interaction between the nodes. This quantity is not easily extracted from Monte-Carlo, or molecular dynamics computer simulations.

A solution to this problem is to calculate the pair potential using a self-consistent field (SCF) theory, as done by Sprakel and coworkers.[14] They used the Scheutjens-Fleer version of the self-consistent field theory(SF-SCF) and modelled one flower-like micelle, with a core/node in the centre of a spherically symmetric system with reflecting boundary conditions on the outside; the so-called cell model. Subsequently they recorded the free energy of the system as a function of the cell size. There is however an obvious problem with determining the pair potential from this free energy. The reflecting boundary conditions imply that images of the central node are encountered in all directions and it is unclear how to calculate a realistic pair potential from this unrealistic particle ordering. Sprakel and co-workers tried to solve this by dividing the free energy by twelve. Because a hexagonal ordering has the greatest number of nearest neighbours, twelve, and is thus most similar to the cell model. It is thus expected that this gives the best estimate for the pair potential.

The first goal of this paper is, therefore, to investigate the suitability of the cell model to obtain pair potentials. We do this by comparing the pair potential calculated with the cell model to that of a pair of nodes on a 3D grid. The advantage of using a 3D grid is that we can model realistic particle configurations, although it takes far more computation time than the cell model. The configurations for which the two pair interactions are compared are: an isolated pair of nodes (IP), a string of Nodes on a line (NoL), and nodes in a simple cubic (cubic primitive: cP) or face centred cubic (FCC) arrangement. The pair interactions are further compared for various lengths of the soluble block N, number of polymers per node f and solvent qualities χ.

The interactions between nodes with triblock copolymers are largely determined by the entropic effect of loop to bridge transitions and the steric repulsion due to the compression of coronal chains. How the associating end-groups are held together is less important. Therefore we simply specify nodes with a predefined volume in which the associative ends of the polymers have

to reside. The telechelics thus either form a loop, starting and ending on the same node, or a bridge, when ending on a different node than the one they started from. We assume that the binding of the end-groups is so strong that the number of free ends is negligible and thus disregard the option that a loose tail is formed, even though some free ends must exist for the gel to relax. This model can be implemented in a cell model, but also for the cP and FCC lattice.

The primary result in the SCF calculations is the free energy of interaction per node $\Delta F(d)$ as a function of the distance to the nearest neighbour d. As the number of neighbours is different in each geometry, we need to extract an effective pair potential $\Delta F_{12}(d)$ from this free energy of interaction to be able to compare the different geometries. Assuming that the pair interactions are pair wise additive, we find $\Delta F_{12}(d)$ by fitting a pair potential such that the sum of the pair interactions of the central node between all contributing node pairs is the same as the free energy of interaction $\Delta F(d)$ for each value of d.

The second goal is to determine whether the assumption that the pair potential is pairwise additive is correct. From the interaction between two isolated nodes (IP), we know the classical pair potential and we can compare this with the pair potential $\Delta F_{12}(d)$ found for the other interaction configurations (NoL, cP, FCC) as well as for the cell model. When pairwise additivity is applicable, all the pair potentials for the different interaction geometries should match. For weak interactions between the nodes (large node distances), the total number of polymer configurations is changed only by a little. In this limit we expect that pairwise additivity is strictly obeyed. For strongly interacting nodes, however, the pairwise additivity will likely break down.

Self-consistent field theory and the molecular model

In this section, a brief introduction is given to the SF-SCF theory of Scheutjens and Fleer.[15–17] The theory was originally designed for the case of polymer adsorption[15,18–22], but found many applications in other fields, such as surfactant self-assembly.[22–24]

The target is to find the volume fraction profiles $\varphi_X(\mathbf{r})$, for any segment type X at coordinate $\mathbf{r}$, such that the total free energy is minimal. To this end, space is divided up in discrete lattice sites. The lattice sites are organised

depending on the symmetry in the system. For the simple cubic and the FCC lattice, parameters are allowed to vary in three dimensions. Then all x, y and z coordinates are specified. One can also recognise lattice layers and average the volume fractions within each layer. Then density gradients only occur in the remaining (e.g. radial) direction, as in the cell model.

Hence, for the simple cubic (cP) and face centred cubic lattice (FCC), the lattice sites are referred to by $\mathbf{r} = (x, y, z)$ coordinates, $x = 1, 2, \ldots M_x$, $y = 1, 2, \ldots M_y$, $z = 1, 2, \ldots M_z$, with periodic boundary conditions in all directions. This is implemented by equating densities just outside the box to its periodic neighbour, e.g. $\varphi(M_x + 1, y, z) = \varphi(1, y, z)$.

For the simple cubic lattice, which was used for the isolated pair (IP), nodes on a line (NoL), and the simple cubic (cP) configurations, a lattice site at coordinate (x, y, z) has neighbours at $(x+1, y, z)$, $(x-1, y, z)$, $(x, y-1, z)$, $(x, y+1, z)$,$(x, y, z+1)$, $(x, y, z-1)$ and the faces on the lattice sites are at 90° angles.

An FCC lattice was used for the face centred cubic (FCC) configuration of nodes. In the FCC lattice, a lattice site has 12 nearest neighbours. A lattice site at coordinate (x, y, z) has neighbours at $(x+1, y, z)$, $(x-1, y, z)$, $(x, y+1, z)$, $(x, y-1, z)$, $(x-1, y+1, z)$,$(x+1, y-1, z)$, $(x, y, z+1)$, $(x, y-1, z+1)$, $(x-1, y, z+1)$, $(x, y, z-1)$, $(x, y+1, z-1)$, $(x+1, y, z-1)$. The x, y and z axis are now at an angle of 60° to each other. The simulation box is thus a parallelepiped with periodic boundary conditions.

The cell model has a spherically symmetric geometry with lattice sites arranged in concentric layers numbered $r = 1, 2, \cdots, M_r$, with layer $r = 1$ at the centre. The number of lattice sites in each layer grows with the layer number as $L(r) \sim r^2$. The mean field approximation is applied within each lattice layer, which means that the content of all lattice sites in a given layer is identical. We have used reflecting boundary conditions by setting all quantities at $r = M_r + 1$ equal to that in layer $r = M_r$. The reflecting boundary condition implies that the distance between two nodes is $d = 2 \times M_r$. It must be stressed that the reflecting boundary conditions are an artificial means to implement the surrounding nodes around a central one and the number of neighbouring nodes varies with the size of the cell model. For the cell model it is also not defined how many neighbouring lattice sites each lattice site has. With the simple cubic lattice in mind we have chosen to have six neighbours for each lattice site, one in the layer above, one in the layer below and four in the same layer. In practice one also needs to take the curvature into account such that the ratio between the number of neighbours in the layer

above and below is the same as the ratio of the volumes of these layers.[25] Below we will focus on the three-gradient SCF approach because this information is not readily available in the literature. The one-gradient equations can be derived from the three-gradient ones and therefore we have reduced the amount of detail for the cell model.

Within the SCF theory molecules consist of a number of segments and each segment has the volume of one lattice site. These segments can be of different types and thus have different properties reflected in the interaction parameters. The polymer molecules are represented by a chain of freely jointed segments numbered $s = 0, 1, 2, \cdots, N + 1$. Segments $s = 0$ and $s = N+1$ are the associative end-groups. The middle N segments form the water-soluble middle block. Subsequent segments, along the chain, have to be on neighbouring lattice sites, but can go in any direction that is consistent with the lattice geometry. The freely jointed chain can therefore cross itself or fold back on itself. This is partially corrected for by imposing an incompressibility constraint, which means that the sum of the volume fractions, of the polymer and the solvent, in each lattice site is exactly one. The segments have to be about a Kuhn length in size for the polymer to be able to fold back. For flexible polymers, like PEO, the length of a segment should thus corresponds to roughly 0.5 to 1 nm.

We want to simulate networks of polymers with associative end-groups. To do this in a computationally inexpensive way, we have simply defined small volumes, called nodes, in which the two terminal segments of all polymers $s = 0$ and $s = N + 1$ are constrained to be. This is depicted schematically in fig. 1b. For the cP and the FCC lattice the nodes are small cubes of $3 \times 3 \times 3$ lattice sites. A chain can choose to put the terminal segments in the same node forming a loop, or place the terminal segments in two different nodes forming a bridge. An illustration of two polymer configurations on the simple cubic lattice is shown in figure 1b.

In the cell model the terminal segments are confined to a sphere with a radius of two layers at the centre of the coordinate system. As long as the polymer does not cross the reflecting boundary, a loop is formed. If the polymer crosses the boundary once, a bridge is formed. If the polymer crosses the reflecting boundary more than once, it is unclear whether a loop or bridge is formed (there is a superposition of the two cases).

The nodes that are formed by the nodes and polymers can be characterized by the length of the soluble middle block N, the number of polymers per node f and the solvent quality for the polymer segments. This solvent

quality is specified by the χ parameter which is defined as the energy required to exchange a solvent and a polymer segment from the pure phases in units k_BT, just as in the Flory-Huggins solution theory.[26] The interactions are accounted for by the usual Bragg-Williams approximation.

We investigated the effect of these characteristic properties of the nodes on the interaction energy between an isolated pair of nodes and for a single node with its mirror images in the cell model. The solvent quality was varied from theta conditions $\chi = 0.5$ to a good solvent $\chi = 0$. The number of chains per node ranged from $f = 1, \cdots, 10$. The polymer length was varied from $N = 12$ to $N = 500$ for the cell model and from $N = 12$ to $N = 100$ for the isolated pair. Each segment is roughly a Kuhn segment long. For a flexible polymer like PEO a Kuhn segment is roughly two monomers.[27] $N = 50$ thus coincides with 100 PEO monomers and a middle block weight of 4400 u. This falls within the range of middle block weights that are studied experimentally which ranges from about 2000 to 35000u.[1,2,4,8,10,13]

To determine whether the interactions are pairwise additive we have calculated an effective pair potential for different node configurations: An isolated pair of nodes (IP), a string of nodes on a line (NoL), a simple cubic configuration (cP) and a face centred configuration (FCC).

As illustrated in figure 2c the isolated pair was modelled by placing two nodes in a rectangular box far enough apart to not interact. By reducing the number of layers in the appropriate direction, the distance through the periodic boundary between the nodes is reduced until both nodes touch each other. For the other configurations (fig. 2a,b,d,e), we used a single node inside the box. For the chain configuration the size of the box was decreased in one dimension only, whereas for the cell model, the simple cubic and the FCC configuration the box was decreased in all three dimensions simultaneously. We calculate a free energy $F(d)$ of the node with the polymers, as a function of the distance d between the nodes through the periodic boundary. The distance d between the centres of the nodes (given in the number of lattice sites) is indicated in figure 2. The free energy of interaction $\Delta F(d)$ is then specified by

$$\Delta F(d) = F(d) - F(\infty) \tag{1}$$

The reference value for the free energy of interaction $F(\infty)$ is the free energy when the nodes are so far apart that the polymers can only form loops.

The calculations are done in a canonical ensemble(n,V,T), and thus with a fixed amount of polymers. Although we change the volume of the box one

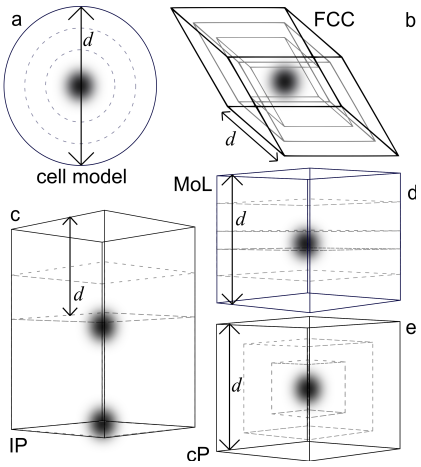

Fig. 2: Overview of how the distance between the nodes was varied for the different node geometries. The grey (dashed) lines indicate smaller box sizes. The grey regions in the middle represent the node with the polymers around it. a) the cell model b) the FCC configuration c) an isolated pair (IP) d) a string of nodes on a line configuration (NoL) e) a cubic (cP) configuration. Periodic boundary conditions are used except for the cell model where a reflecting boundary is used.

can imagine that there is an additional volume such that the total volume remains constant. As this volume only contains pure solvent for which the chemical potential is defined as 0, it does not contribute to the free energy. The appropriate characteristic function is thus the Helmholtz energy. Here our interest is in the free energy for the system wherein the ends of all polymer chains are constrained to be on the node positions which are conveniently collected in the set of n coordinates, $\{\mathbf{r}_n\}$, exactly specified by the input of the calculations.

Central in the SCF theory is a mean field free energy which is a functional of two complementary distributions, the volume fraction profile of the segments and a segment potential profile. This mean field free energy can be written in the generic form[17]:

$$F = -\sum_{\mathbf{r}}\sum_{X}\varphi_X(\mathbf{r})u_X(\mathbf{r}) + \sum_{\mathbf{r}}\alpha(\mathbf{r})\left(\sum_{X}\varphi_X(\mathbf{r}) - 1\right) + U([\varphi]) - \ln Q([u]) \tag{2}$$

In which $\varphi_X(\mathbf{r})$ is the volume fraction and $u_X(\mathbf{r})$ is the segment potential of segments type X at position $\mathbf{r}$. In the second term $\sum_{\mathbf{r}} \alpha(\mathbf{r}) \left(\sum_X \varphi_X(\mathbf{r}) - 1\right)$ we use the the Lagrange multiplier method to ensure that the sum of the volume fractions is one in all lattice sites. The interaction energy $U([\varphi])$ between the segments depends on the volume fraction distribution. It is, for the Flory-Huggins equation of state, given by:

$$U([\varphi]) = \sum_{\mathbf{r}} \sum_{X} \sum_{Y} \chi_{XY} \varphi_X(\mathbf{r}) \langle \varphi_Y(\mathbf{r}) \rangle \tag{3}$$

Here χ_{XY} is the (Flory-Huggins) interaction energy between segments X and Y and $\langle \varphi_Y(\mathbf{r}) \rangle$ is the average volume fraction of segment type Y in the sites around $\mathbf{r}$:

$$\langle \varphi_Y(\mathbf{r}) \rangle = \frac{1}{Z} \sum_{\mathbf{r}'} \varphi_Y(\mathbf{r}) \delta_{|\mathbf{r}'-\mathbf{r}|-1} \tag{4}$$

where the Kronecker $\delta_{|r'-r|-1} = 1$ when $|\mathbf{r}' - \mathbf{r}| - 1 = 0$ and zero otherwise. Z is the number of neighbours of the lattice site at r. Finally, $Q([u])$ is the partition function which depends on the segment potentials $u_X(\mathbf{r})$.

In the mean field Ansatz the partition function of the system can be rewritten in terms of single molecule partition functions q_i

$$Q = \prod_i \frac{q_i^{n_i}}{n_i!} \tag{5}$$

Wherein n_i is the number of molecules of type i. The partition function can be evaluated efficiently by using the freely jointed chain model. Within this model q_i is found by $q_i = \sum_{\mathbf{r}_n} G_i(\mathbf{r}_n, N+1|\{\mathbf{r}_n\}, 0)$. In this case the summation can be limited to the sum over the set of coordinates $\mathbf{r}$ that lie within the nodes. Here $G_i(\mathbf{r}_n, N+1|\{\mathbf{r}_n\}, 0)$ is called the end point distribution function and is effectively the sum of the statistical weights of all chain conformations ending at the node position $\mathbf{r}_n$ with segment $s = N + 1$ while segment $s = 0$ can be located within any node in the system.

All conformations that contribute to the end point distribution function at a location $\mathbf{r}$ will have the same Boltzmann weight for the last segment $s = N + 1$. This term $G_i(\mathbf{r}, N + 1)$, which is equal to $e^{-u(\mathbf{r},N+1)}$ when $\mathbf{r} \in \{\mathbf{r}_n\}$ and zero otherwise, can thus be moved outside the summation. Since the chain must have come from one of Z adjacent lattice sites, the remainder of the summation can be written as a summation of the end-point

distribution function, of the chain without the last segment, on adjacent sites multiplied with the fraction of the paths $\frac{1}{Z}$ from adjacent site $\mathbf{r}'$ that go from $\mathbf{r}'$ to site $\mathbf{r}$.

$$G_i(\mathbf{r}, N+1|\{\mathbf{r}_n\}, 0) = G_i(\mathbf{r}_n, N+1)\frac{1}{Z}\sum_{\mathbf{r}'} G_i(\mathbf{r}', N|\{\mathbf{r}_n\}, 0)\delta_{\mathbf{r}'-\mathbf{r}} \qquad (6)$$

This equation is known as the propagator, because it relates walks that are $N+1$ steps long to one that is N segments long. This process can be repeated, that is we can relate $G_i(\mathbf{r}, N|\{\mathbf{r}_n\}, 0)$ to a summation over $G_i(\mathbf{r}', N-1|\{\mathbf{r}_n\}, 0)$, etcetera, until $G_i(\mathbf{r}, 0|\{\mathbf{r}_n\}, 0)$ is reached. For this last one, we have $G_i(\mathbf{r}, 0|\{\mathbf{r}_n\}, 0) = G_i(\mathbf{r}_n, 0) \equiv e^{-u(\mathbf{r}_n,0)}$ for all node-positions ($\mathbf{r} \in \mathbf{r}_n$), while the end-point distribution $G_i(\mathbf{r}, 0|\{\mathbf{r}_n\}, 0) = 0$ for all remaining lattice sites $\mathbf{r} \notin \{\mathbf{r}_n\}$.

Hence, the partition function q_i can be obtained by starting the calculation at $G(\mathbf{r}_n, 0|\{\mathbf{r}_n\}, 0)$ and from these calculate $G_i(\mathbf{r}, 1|\{\mathbf{r}_n\}, 0)$ and further on, via $G_i(\mathbf{r}_n, s|\{\mathbf{r}_n\}, 0)$, till $G_i(\mathbf{r}_n, N+1|\{\mathbf{r}_n\}, 0)$ is reached, that is the propagators are executed in the reverse order as introduced above.

The end point distribution functions can further be used to determine the local volume fractions of the segments $\varphi_i(\mathbf{r}, s')$. More specifically, $\varphi_i(\mathbf{r}, s')$ is proportional to the end-point distribution functions that collect all statistical weight of those conformations that pass through coordinate $\mathbf{r}$ with segment $s = s'$. It is the product of the two complementary propagators of the chain fragments, one leading from segment $s = 0$ to segment $s = s'$ and another one from segment $s = N+1$ to segment $s = s'$.

$$\begin{aligned}\varphi_i(\mathbf{r}, s') &= C_i\frac{G_i(\mathbf{r}, s'|\{\mathbf{r}_n\}, 0)G_i(\mathbf{r}, s'|\{\mathbf{r}_n\}, N+1)}{G_i(\mathbf{r}, s')} \\ &= C_i\frac{G_i(\mathbf{r}, s'|\{\mathbf{r}_n\}, 0)G_i(\mathbf{r}, N-s'+1|\{\mathbf{r}_n\}, 0)}{G_i(\mathbf{r}, s')} \qquad (7)\end{aligned}$$

Because the Boltzmann weight of segment $s = s'$ is in both end point distribution functions we need to correct by division with $G_i(\mathbf{r}, s')$. In the second line we have rewritten the partition function. Because the polymer is symmetrical we only need to evaluate the propagator in one direction and can thus save computation time. The normalization constant C_i is easily found as the ratio between the number of chains n_i and the single chain partition function q_i.

$$C_i = \frac{n_i}{q_i} \qquad (8)$$

The overall volume fraction distribution of polymers is found by a summation over the segments

$$\varphi_i(\mathbf{r}) = \sum_{s=0}^{s=N+1} \varphi_i(\mathbf{r}, s) \tag{9}$$

The distribution of the monomeric solvent simply follows from the Boltzmann weight

$$\varphi_S(\mathbf{r}) = C_S G_S(\mathbf{r}) = C_S e^{-u_S(\mathbf{r})} \tag{10}$$

When the segment potentials are normalized to zero in the bulk, it is easily shown that $C_S = 1$.

Now we still need a method to determine the segment potentials $u_X(\mathbf{r})$. Because the self-consistent solution we are looking for is the one with the lowest free energy. We need to optimize the free energy to the parameters $u_X(\mathbf{r})$, $\varphi_X(\mathbf{r})$ and $\alpha(\mathbf{r})$. This optimization then directly leads to the methods for determining the segment potentials from the segment volume fractions and *vice versa*. The optimization with respect to the volume fractions gives

$$\frac{\partial F}{\partial \varphi_X(\mathbf{r})} = -u_X(\mathbf{r}) + \sum_Y \chi_{XY} \langle \varphi_Y(\mathbf{r}) \rangle + \alpha(\mathbf{r}) = 0 \tag{11}$$

which specifies how to compute the segment potentials in the SCF machinery.

$$u_X(\mathbf{r}) = \sum_Y \chi_{XY} \langle \varphi_Y(\mathbf{r}) \rangle + \alpha(\mathbf{r}) \tag{12}$$

The optimization of the free energy with respect to the Lagrange parameter $\alpha(\mathbf{r})$ leads to the rule that we need to obey to the constraint $\sum_X \varphi_X(\mathbf{r}) = 1$. The optimization of the free energy with respect to the segment potentials gives the rule how to compute the volume fraction distribution from the potentials:

$$\frac{\partial F}{\partial u_X(\mathbf{r})} = -\frac{\partial \ln Q}{\partial u_X(\mathbf{r})} - \varphi_X(\mathbf{r}) = 0 \tag{13}$$

$$\varphi_X(\mathbf{r}) = -\frac{\partial \ln Q}{\partial u_X(\mathbf{r})} \tag{14}$$

This method for determining the volume fractions is however computationally less efficient than the previously described method. We have thus used eqn. 9 to calculate the volume fractions.

Now only the parameter $\alpha(\mathbf{r})$ remains to be defined. There is no clear way how to choose this alpha, but all possibilities should have in common that the value of α should increase when $\sum_X \varphi_X(\mathbf{r}) > \mathbf{1}$ and decrease when $\sum_X \varphi_X(\mathbf{r}) < \mathbf{1}$. We choose to update alpha at each iteration step as:

$$\alpha_{\text{new}}(r) = \alpha_{\text{old}}(r) + \eta(1 - \frac{1}{\sum_X \varphi_X(\mathbf{r})}) \tag{15}$$

where η is a regularisation parameter which is taken small enough so that the equations do not diverge (typically $\eta = 0.3$ gives a stable scheme. In any case, we do not terminate the iterations until a fixed point is reached for all $\alpha(\mathbf{r})$ values.

The above set of equations fully specifies how to compute the potentials from the volume fractions and *vice versa*. The numerical solution is routinely calculated with a Hessian-free minimization method. For the calculations in this paper the L-BFGS method[28] was used. We obtained at least 7 significant digits for the potentials and for the volume fraction distributions. Using these we can evaluate the free energy we need in equation 1, which is at the basis of the evaluation of the pair potentials.

Now that the free energy of the system is known we can determine an effective pair potential $\Delta F_{12}(d)$ for the different geometries. The effective pair potential is the pair potential that will reproduce the free energy of interaction $\Delta F(d)$ when all the interactions between pairs of nodes are summed together. We thus assume that the interactions are pair wise additive to determine $\Delta F_{12}(d)$. If this is indeed the case we should find the same $\Delta F_{12}(d)$ for all configurations. There are however many reasons why the interaction may not be pair wise additive. E.g. one node may be in between two other nodes blocking some of the bridging conformations between them. Therefore one of our targets is to quantify this loss in pair wise additivity.

$\Delta F_{12}(d)$ has been calculated for the four different particle configurations. The idea to find the pair potential for a given interaction geometry is the following; In a given interaction geometry it is trivial to find the number of neighbours at a given distance from the central node. Let us label these neighbours by $k_1 = 1, \cdots K_1$, where K_1 is the number of nearest neighbours. Similarly we number the next nearest neighbours as $k_2 = 1, \cdots, K_2$, etcetera. The distance to the central node for these neighbours is given by d_{k_1} for the nearest neighbours and d_{k_2} for the next nearest neighbour, etcetera. Then

assuming that for this effective pair potential the pairwise additivity holds, we should recover the total interaction energy by summing the pair interaction over all the contributions of the neighbours:

$$\Delta F(d) = \sum_{k_1=1}^{K_1} [\Delta F_{12}(d_{k_1})] + \sum_{k_2=1}^{K_2} [\Delta F_{12}(d_{k_2})] + \cdots \tag{16}$$

We continue to account for the neighbours further away until they no longer contribute to the summation. The effective pair potential was calculated iteratively from the known $\Delta F(d)$ for a given interaction geometry. An initial guess for the effective pair potential $\Delta F_{12}(d)$ is made by dividing the total interaction potential by the number of nearest neighbours. Subsequently, the contribution from the neighbours further away is calculated based on this potential. These contributions are then subtracted from the total interaction potential. The remainder of the potential is then again divided by the number of nearest neighbours to get a new estimate of $\Delta F_{12}(d)$. This is repeated until $\Delta F_{12}(d)$ remains constant. Because the next nearest neighbours may lie at non-integer distances a cubic spline function was used to interpolate between the data points of $\Delta F_{12}(d)$. Obviously, for the IP geometry we find $\Delta F_{12}(d) = \Delta F(d)$ because there is just one neighbour involved.

For the cell model the effective pair potential cannot be calculated in this manner and we have simply divided $\Delta F(d)$ by twelve, because this is the number of nearest neighbours in an FCC lattice which is the most similar to the cell model.

Results and Discussion

We subdivide the results section into two parts. First we present the results for the one-gradient calculations, that is for the classical cell model. These calculations are inexpensive as they typically take less than a tenth of a second of CPU time for each distance. Most of these results are at least qualitatively known in the literature and are reproduced here for comparison. In the second part we will present results of the three-gradient calculations with a focus on the results for the isolated pair. These calculations take on the order of one minute of CPU time for each distance and determine the free energy with an error less than 0.01 k_BT within the assumptions of the model used here. At the end of this section we will focus on the pairwise

additivity of the pair potential and show the results for the NoL, cP and FCC configurations.

Cell model results

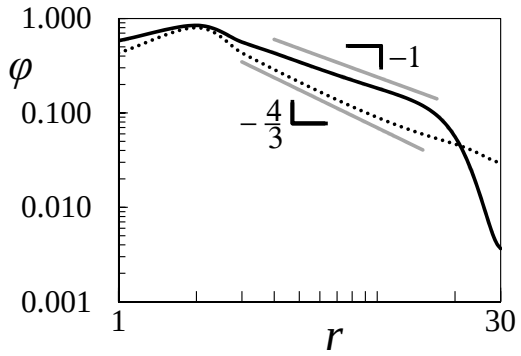

Fig. 3: Radial polymer volume fraction profile around a node in the cell model. $N = 500$, $f = 10$. The continuous line is for theta solvent $\chi = 0.5$ whereas the dotted line is for good solvent, $\chi = 0$. The slope of the power-law region of the profile is indicated, which is -1 for theta solvent and $-\frac{4}{3}$ for good solvent.

In figure 3 results for the radial density profiles, calculated with the cell model are presented in double logarithmic coordinates for the case $N = 500$, $f = 10$ and, $\chi = 0.5$ and $\chi = 0.0$. In the central region $2 < r < 10$ where the curvature is important, the polymer density decays like a power law. The exponents are very close to those for star polymers which are $-4/3$ in a good solvent and -1 in a theta solvent.[29] The profiles found here therefore look very similar to those reported by Wijmans et al.[30] for star polymers. The region for which the power law behaviour is observed is small as the polymers are relatively short. For $\chi = 0.5$ the edge of the polymer brush is reached at $r \approx 15$ where the polymer density decreases exponentially. As the thickness of the corona layer in good solvent is larger than that of the theta solvent, the profiles cross each other around $r = 20$. The profile for the good solvent hits the upper boundary at $r = 30$ and crosses this boundary with zero slope (this is imposed by the boundary condition). The finite concentration at the boundary implies that bridges are formed. In the theta-solvent $\chi = 0.5$ the reflecting boundary is still far from the edge of the polymer brush and a

negligible number of bridges is present. For $\chi = 0$ and $r > 15$ the polymer density is higher than expected from the power law behaviour. This is due to polymer loop conformations that in a free micelle would extend beyond the edge of the cell are now folded back into the cell.

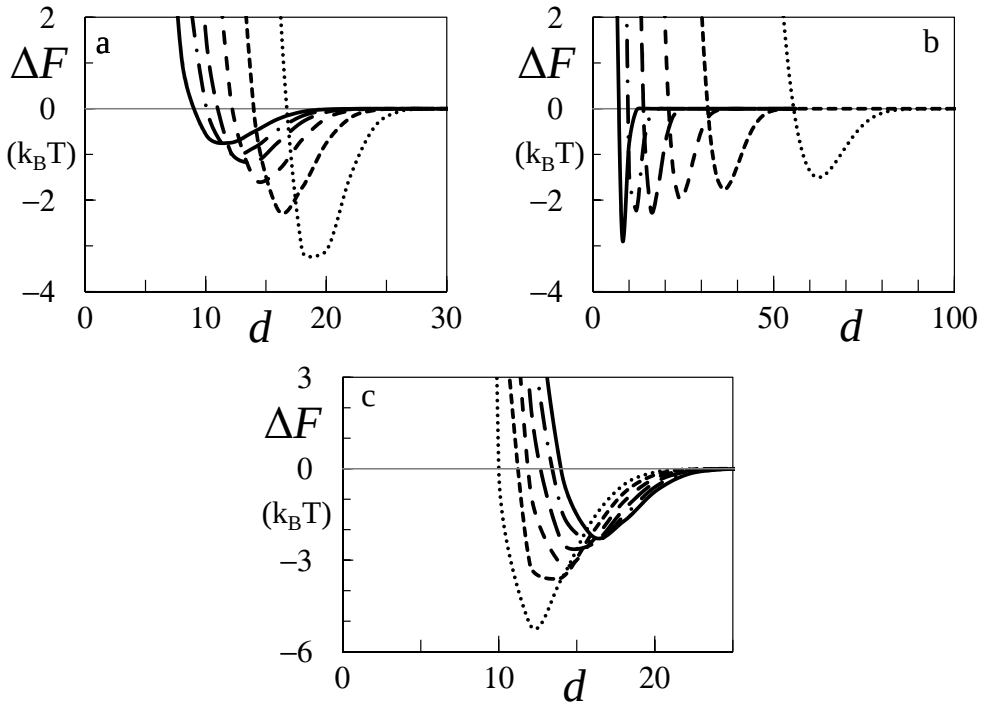

Fig. 4: Free energy of interaction ΔF for the cell model as a function of the distance $d = 2 * M_r$ between the node and its mirror image. a) $N = 50$, $\chi = 0$ and the number of polymers per node ranging from left to right : $f = 1$ (—), 1.5, 2, 3, 5, 10 ($\cdots$) b) $\chi = 0$, $f = 5$, and the chain length varied from left to right: $N = 12$ (—), 25, 50, 100, 200, 500 ($\cdots$). c) $N = 50$, $f = 5$, and varied solvent quality: from left to right: $\chi = 0.5$ (theta solvent, $\cdots$), 0.4, 0.3, 0.2, 0.1, 0 (good solvent, —).

The dimensionless free energy of interaction $\Delta F(d)$ is computed in the cell model for different values of the cell size M_r. In figure 4 we give a summary of the interaction free energy curves for the cell model. The default system has chains with a length of 50 segments, $N = 50$, five chains per node, $f = 5$, and a good solvent, $\chi = 0$.

In figure 4a the effect of the variation in the number of polymers per node is presented, in figure 4b we show the result for the variation of the chain length and finally in figure 4c the solvent quality was varied. At large distances, $d \to \infty$, the free energy of interaction is zero. As soon as the coronas 'touch' each other, bridges form and an attraction is found. Hence, ΔF becomes negative. At small values of d the corona layers are strongly compressed and steric repulsion is found. The interaction curve can be characterized by, the depth, width and position of the attractive well. Although the steepness of the repulsion also varies, it is usually so steep that the range over which the micelle behaves as a soft particle rather than a hard sphere is small and the excluded volume thus does not change much due to the varying steepness of the repulsion. Because there can only be an integer number of layers in the cell model, the free energy of interaction is only available at even values of d. This is why the curves appear somewhat kinky. In reality the interaction curves should of course be smooth.

In figure 4a the dependence of the free energy of interaction on the number of chains per node, f, is presented. The depth of the attractive well increases and both the minimum and the onset of the steric repulsion occur at greater distances d with an increasing f. Both trends are easily explained. The attraction is due to the transformation of loops into bridges and the more bridges can form the deeper the minimum. The depth of the minimum however does not scale linearly with the number of arms but roughly with $\Delta F_{min} \sim f^{0.65}$. Due to the limited number of points the depth of the well is not determined accurately enough to conclude that there is power law behaviour.

A larger number of chains on a node also increases the height of the corona and the micelles will thus attract each other at greater distances. An increase in the number of polymers per node however also leads to an increased polymer density in the corona and thus an earlier onset of the steric repulsion. Therefore the minimum shifts to larger separations d. Fitting of the position of the minimum as a function of the number of arms gives to a good approximation $d_{\min} \propto f^{0.2}$, which is expected from the Daoud Cotton model.[29] Below in figure 9 we elaborate more on the depth of the interaction curve as a function of f.

The chain length dependence for the free energy of interaction is presented in figure 4b. The position of the minimum is found to scale with the corona thickness which in turn depends on the length of the polymers. In the limit of large N values $d_{\min} \propto N^{3/5}$ is found to a good approximation, which is

in accordance with the Daoud Cotton model.[29] The depth of the interaction minimum is, on the other hand, a weak function of the chain length and it decreases with increasing chain length. We further observe a broadening of the well. We will return to this point in figure 10.

The third variable that is relevant to investigate is the solvent quality. As can be seen in figure 4c the relevant features of the free energy of interaction systematically shifts to larger d values when the solvent quality improves. As mentioned before, the minimum is generated by steric repulsion at short distances and attraction at larger distances due to the loop to bridge transitions. At large distances the attraction is not much affected by the solvent quality. The main effect is the onset of the repulsion which occurs at larger distances when the solvent quality is better. As illustrated by the radial volume fraction profiles in fig. 3, the corona is more swollen in a good solvent. This swelling of the corona is due to the increased value of the segment virial coefficient $v = 1 - 2\chi$, which specifies the repulsion between segments that encounter each other in the corona. The overlap between the coronas is more repulsive the larger the virial coefficient is. The position at which the repulsion is larger than the attraction will thus shift to greater distances d. The width and depth of the well will thus decrease and the minimum of the interaction curve shifts outward.

Three-gradient models

It is illustrative to first discuss some typical examples of the polymer density as found in the three-gradient calculations. Figure 5 shows a polymer density plot for a cross section taken such that the plane crosses the nodes through their centres, for a) the isolated pair (IP), b) a series of nodes on a line and c) the cP arrangement of nodes. In the cross sections the square lattice is clearly visible. A higher polymer density is indicated by a darker colour. The polymer density for the IP (figure 5a) shows that the polymer is arranged slightly asymmetrically around the two nodes. Because bridges can be formed, there are more polymer conformations possible between the nodes and the polymer density is thus higher. Similar effects are seen for the string of nodes on a line (figure 5b). Halfway in between the nodes, the polymer density is a bit higher than on comparable distances in the other directions. Also in the simple cubic arrangements (figure 5c) we see an inhomogeneous distribution around the node. In the contact regions the polymer density is a bit higher due to the bridging that takes place.

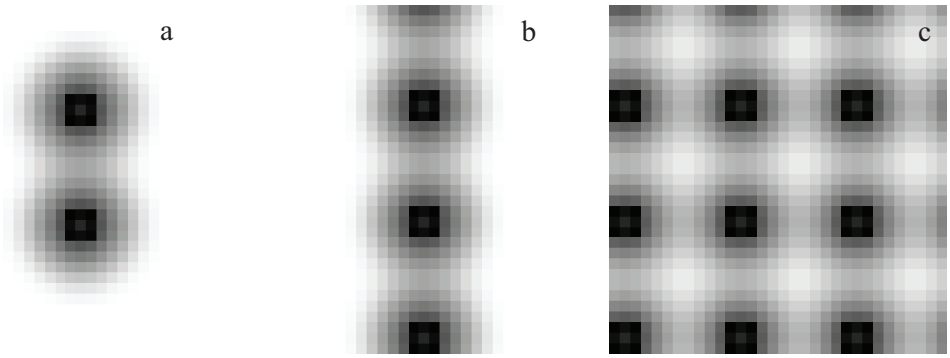

Fig. 5: A cross section through a three-gradient density profile of the polymer segments. a) an isolated pair (IP), b) a line of nodes (NoL), c) a simple cubic (cP) arrangement of nodes. The cross section is taken through the centres of the nodes. $N = 50$ $\chi = 0.5$, $f = 5$. The dark areas indicate a high polymer density.

Just as in the cell model, we can determine the volume fraction, as a function of the distance from the centre of an isolated node, for the three-gradient calculations. In figure 6 radial profiles are shown for micelles, with $N = 50$ and $f = 10$, in the cell model, on a cubic lattice and on an FCC lattice, for both good $\chi = 0$ (panel a) and theta $\chi = 0.5$ (panel b) solvents. The curve for the cP and the FCC lattice was taken through the centre of one of the faces of the cube/parallelepiped. Because the density at the corners of the cube shaped node was higher than in the middle of the faces, the amount of polymer that would be found if one integrated over the polymer density is a bit lower for the cP lattice than for the cell model. Because the distance between the centres of the nodes was kept the same for the cP and FCC lattice, the volume of a lattice site in the FCC lattice is smaller than in the cubic lattice. As a consequence there are more lattice sites within a certain radius of the centre of the node in the FCC lattice than in the cP lattice and the polymer density for the FCC lattice will thus be lower than that of the cP lattice.

As the middle blocks try to move outward, to reduce the steric repulsion between them, the end-groups are pulled to the surface of the node. This increases the polymer concentration at the surface and lowers the polymer

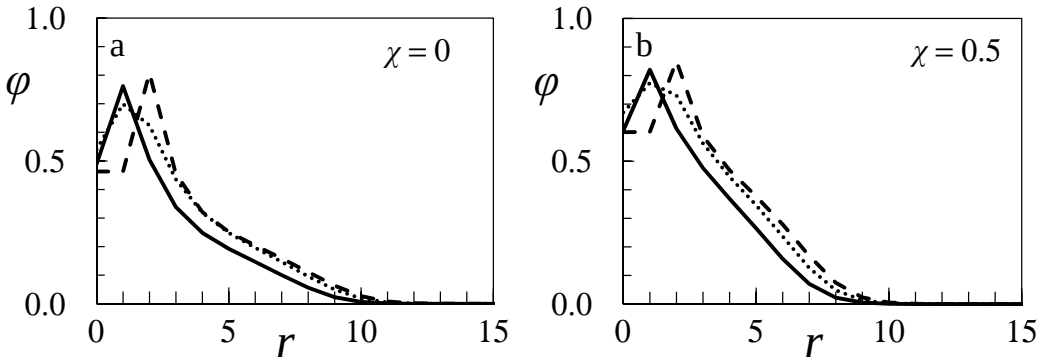

Fig. 6: The volume fraction of the polymer as a function the distance r in lattice sites from the centre of the node for $\chi = 0$ (a) and $\chi = 0.5$ (b). $f = 10$, $N = 50$. FCC lattice (—), cell model (- - -), simple cubic($\cdots$).

concentration in the centre of the node, as seen in figure 6. As expected, the profiles in figure 6 are very similar. This indicates that the cell model is giving a reasonable prediction for the typical distribution of segments around a node. As the details of the radial profiles were already discussed for the cell model, see fig. 3, we will not repeat them here. The polymers are too short to be able to clearly see power law behaviour in fig. 6.

When two nodes are sufficiently close to each other, bridges may form. It is of interest to quantify the number of bridges, which can be computed similarly as for the evaluation of bridges between two surfaces[19]. We realise that the number of bridges is given by the total number of chains minus the number of loops. The latter can simply be computed from evaluating the number of chains that start and end at the same node. This is done by recalculating the single chain partition function q_i, with just one of the nodes present and without adjusting the segment potentials. With $n_i = C_i q_i$ and the C_i from the calculation with all nodes present, the number of polymers in a loop configuration on that node is determined.

The evaluation of the number of bridges in the cell model is problematic as it is not clear whether a loop or bridge is formed when the polymer crosses the periodic boundary more than once. For a pair of isolated nodes the mentioned procedure is easily implemented which leads to the number of bridges for a given position of the two nodes. Throughout this paper the nodes are oriented along either the x or y or z-direction in the lattice, so

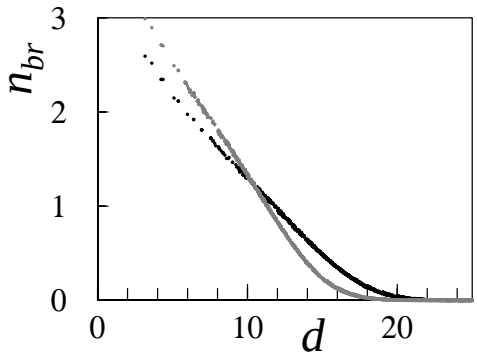

Fig. 7: The number of bridges $n_{\rm br}$ between a pair of isolated nodes, on a cubic lattice for $\chi = 0$ to $\chi = 0.5$, as a function of the distance between the centres of the nodes d. The black dots belong to $\chi = 0$ and the grey dots belong to $\chi = 0.5$; $f = 5$ and $N = 50$.

that the distance between the nodes is an integer number of lattice sites. However, the nodes may also be oriented differently with respect to the lattice directions. Information on the number of bridges as a function of the distance between the nodes for arbitrary orientation of the nodes in the lattice can give information on the presence or absence of a lattice artefact in our calculations. In short, we have generated a large number of random positions for the pair of nodes in our system and for each of these positions we have evaluated the number of bridges $n_{\rm br}$. In figure 7 the number of bridges between an isolated pair of nodes $n_{\rm br}$ is shown for the default conditions for both $\chi = 0$ and $\chi = 0.5$. The number of bridges scales with the amount of the polymer loops at the mirror plane between the micelles (not shown). For each point where a polymer in a loop conformation crosses this mirror plane, the mirror image of the second part of the conformation forms a new bridging conformation. As the number of polymers that cross the mirror plane decreases almost linearly with increasing distance between the nodes, the number of bridges also decreases linearly with increasing distance d. This is especially clear for $\chi = 0.5$. Even though the points in figure 7 do not lie perfectly on a line the deviations are small, proving that the orientation of the nodes relative to the grid has little influence on the number of bridges.

We can evaluate the number of bridges also in more complicated configurations of the nodes, however, these calculations may become involved as soon as more particles are involved (NoL, cP or FCC), because we should dis-

tinguish bridges between nearest neighbours from those between next nearest neighbour and so forth. As the comparison with the cell model is not straightforward, we will not further analyse the number of bridges and rather focus on the free energy of interaction, which is the result of the bridging attraction and steric repulsion.

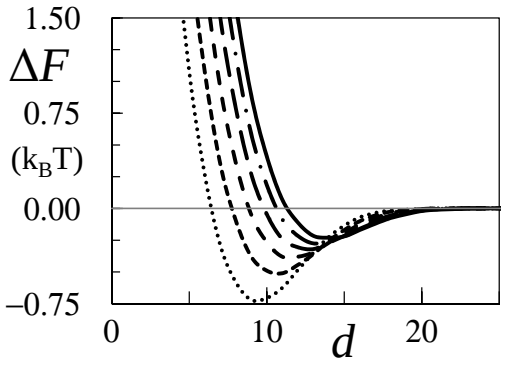

Fig. 8: The interaction free energy ΔF between a pair of isolated nodes on a cubic lattice for χ ranging from 0 to 0.5 in steps of 0.1. The continuous line belongs to $\chi = 0$ and the dotted line to $\chi = 0.5$; $f = 5$ and $N = 50$.

We have used the simplest particle configuration for which bridge formation occurs, the isolated pair(IP) on a cubic lattice, to study how the free energy of interaction depends on the length of the polymers N, the number of polymers per node f and the Flory interaction parameter χ. The interaction curves, for different values of the solvent quality χ, are shown in figure 8. In this case there were 10 polymer chains, 5 per node ($f = 5$) and each polymer had $N = 50$ segments. With decreasing distance, the loop to bridge attraction is expected to increase as there are more bridging conformations (see fig. 7). The steric repulsion however also increases with decreasing distance because the corona layers are compressed. The resulting well depth is therefore an interplay with the strengths and the ranges of these two contributions. For a good solvent the corona layer is more extended and the repulsive contribution becomes longer ranged which causes the depth of the well to become less deep with increasing solvent quality.

Qualitatively the interaction curves are similar to those of the cell model. With increasing values of χ, the trend of increasing well depth and a decreasing distance at which the minimum of the interaction is observed, is

clearly visible and the results qualitatively compare well to the result of the cell model discussed above in fig. 4c. Quantitative differences are obvious. Most importantly the absolute value for the free energy of interaction ΔF is much smaller for the IP case. This is easily explained, for the IP there is just one direction in which a bridge can be formed whereas for the cell model a bridge can be formed in all directions. As shown in fig 5a the chains remain roughly isotropically distributed around the node when the other node is in its vicinity. As a result only a few chains can form bridges and the free energy of interaction remains modest. Another quantitative difference is the observation that the interaction curves are shifted to shorter distances for the IP as compared to the cell model and the steric repulsion is less steep. This is due to the fact that for the IP the chains have room to move out of the gap between the nodes when the nodes are forced towards each other. This is not possible in the cell model, the cP and the FCC cases.

Next we choose to focus on the depth of the minimum in the free energy of interaction curve. We use the notation $\Delta F_{\min}$ and note that the negative value of this quantity is kept to remind ourselves that there is an attractive well.

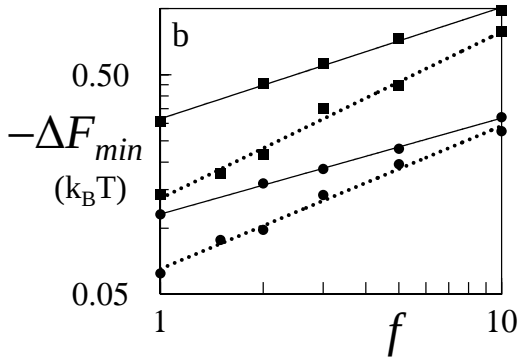

Fig. 9: The depth of the attractive well $\Delta F_{\min}$, as a function of the number of chains per node f, on a double logarithmic scale, for the cell model ($\cdots$) and the isolated pair(—) for $\chi = 0$ (Spheres) and $\chi = 0.5$ (Squares). For the the cell model $\frac{1}{12}\Delta F_{\min}$ is plotted. The lines are the power law fits. $N = 50$

For the IP interaction geometry we collected $-\Delta F_{\min}$ as a function of the number of chains per node f. In figure 9 this dependence is shown in double logarithmic coordinates. Even though the range over which we

can change f is limited, it is found that the depth of the attractive well increases with f as a power law. The exponents found range from 0.44 for $\chi = 0$ to 0.51 for $\chi = 0.5$. Semenov et al. did predict power law behaviour for this dependence, but the expected coefficients ranged from 0.3 to 0.33 for $\chi = 0$ to 0.5.[6] Possibly, the relatively short chain length, $N = 50$, has influenced the coefficients. These results can be compared to the cell model results presented in fig. 4a. Also for the cell-model power law dependence is found and the results are presented in fig. 9's dotted lines. In this case the free energy of interaction was divided by the expected surrounding of 12, which corresponds to a FCC surrounding. For the cell model the power law coefficients ranged from 0.65 for $\chi = 0$ to 0.76 for $\chi = 0.5$ which is significantly larger than for the IP geometry. The larger coefficient for the cell model is probably due to the reduced steric hindrance between the bridge forming chains compared to the IP geometry. For the IP geometry there is only one way to form bridges and if multiple bridges are formed there will be steric hindrance between them. In the cell model bridges can however be formed in any direction and there is thus no strong steric repulsion between bridge forming chains.

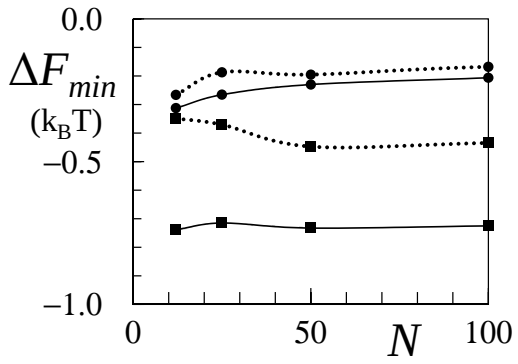

Fig. 10: The depth of the attractive well $\Delta F_{\min}$ as a function of the chain length for a good solvent $\chi = 0$ (spheres), and a theta solvent $\chi = 0.5$ (squares) both for the cell model for which $\frac{1}{12}\Delta F_{\min}$ is given $(\cdots)$ as well as for the IP geometry(—) ; $f = 5$.

The effect of the polymer chain length on the depth of the attractive well, for the IP and the cell model, is shown in figure 10. (For the cell model the free energy of interaction was again divided by 12). For the IP there is hardly a chain length dependence at $\chi = 0.5$, for $\chi = 0.3$ (not shown) and $\chi = 0$

there is a weak decrease of the well depth with N, which seems to level off at large values of N. The weak chain length dependence is unexpected as the total number of bridges that can form is given by f and this quantity is fixed. For the cell model the distance to a mirror image of the node could only be changed by 2 lattice sites at a time. This reduces the accuracy with which the minimum can be determined, especially for the chains of 12 and 25 segments. It is thus not clear whether the decrease of the well depth with increasing length in a theta solvent is significant for the cell model, although the well depth seems to decrease by about 10% going from $N = 50$ to $N = 500$. For a good solvent the cell model shows the same trend as the IP, as can be seen in figure 4b.

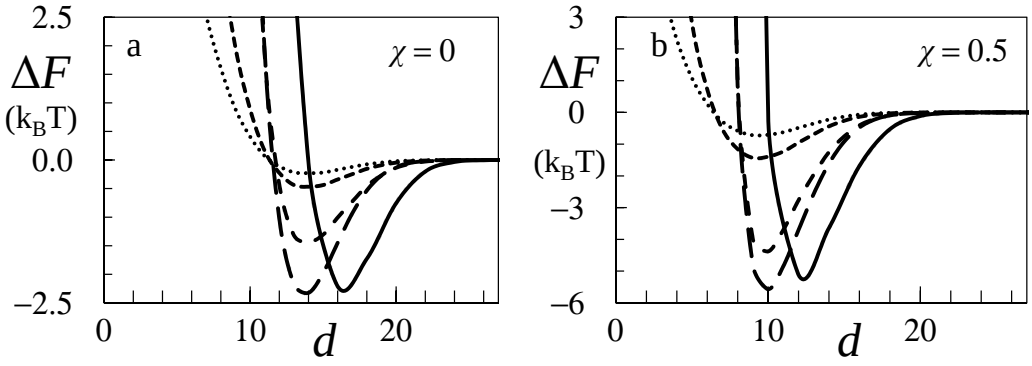

Fig. 11: The free energy of interaction per node as a function of the distance d between nodes measured in lattice sites, for $f = 5$ and $N = 50$. a) $\chi = 0$ (b) $\chi = 0.5$. Results are collected for different interaction modes. From the dotted line to the continuous line: IP, NoL, cP, FCC and the cell model.

Let us now compare the results for the free energy of interaction between the nodes, for the cell model, the IP, the NoL, the cP and the FCC configurations. In Figure 11 the interaction energy per node is presented for these interaction geometries with $f = 5$ and $N = 50$, for a good solvent (panel a) and a theta solvent (panel b). In these calculations we made no corrections for the number of neighbours per node. Therefore the absolute value of the free energy of interaction differs a lot between the configurations. Below we will present the corresponding 'effective pair potentials' which correct for the number of neighbours. For the cell model the attractive well is shifted to greater distances. This is because the number of neighbouring nodes in-

creases with the square of the distance, whereas the number of nodes remains constant for all other particle configurations. This gives an extra $\log d^2$ term to the attraction, resulting in an increased long range attraction for the cell model.

At a smaller cell size a neighbouring node is seen in all directions through the reflecting boundary conditions, there is thus a strong steric repulsion between the node and its mirror images when the cell size is reduced. Hence, the onset of the repulsive part of the interaction occurs at greater distances as well. The minima are at a shorter range for $\chi = 0.5$ than for $\chi = 0.0$, which is expected from the reduced swelling at $\chi = 0.5$.

For the IP, the NoL and cP interaction geometries, the depth of the attractive well is proportional to the number of nearest neighbours. For the FCC configuration the depth of the attractive well is less than the depth expected from the number of nearest neighbours. About $\frac{5}{6}$ of the expected value for $\chi = 0$ and $\frac{2}{3}$ for $\chi = 0.5$. For the simple cubic configuration a deeper attractive well would be expected as well, because there are still twelve next nearest neighbours which are near enough to form a bridge. Assuming the interactions are the same as for an isolated pair, the sum of all these interactions should give a potential well deeper than the one found here for the cubic and the FCC configuration.

In figure 12 we show the effective pair potentials $\Delta F_{12}(d)$ for the different interaction geometries, again for the two solvent qualities: good solvent, panel (a) and theta solvent panel (b). These pair potentials were extracted from the interaction free energy curves presented in figure 11. To compare these effective pair potentials with the free energy per node from the cell model, the free energy in the cell model was divided by 12 assuming that there are twelve nearest neighbours as in an FCC or a hexagonal configuration. The same approach to obtain a pair potential from the cell model was used by Sprakel et al.[7]

As can be seen in figure 12, the attractive part of the effective pair interaction is practically the same for the IP and the NoL configurations, especially for the good solvent case for which the curves overlap. The repulsion between the nodes in the NoL configuration increases more rapidly for $\chi = 0.5$, compared to the IP, because there is less space for the chains to escape to in the NoL configuration. There is a large difference between the IP and the configurations where the node is surrounded by other nodes in all directions, the cell model, the cP, and the FCC configuration, especially for $\chi = 0.5$. The repulsion occurs at larger distances and the potential well is less deep

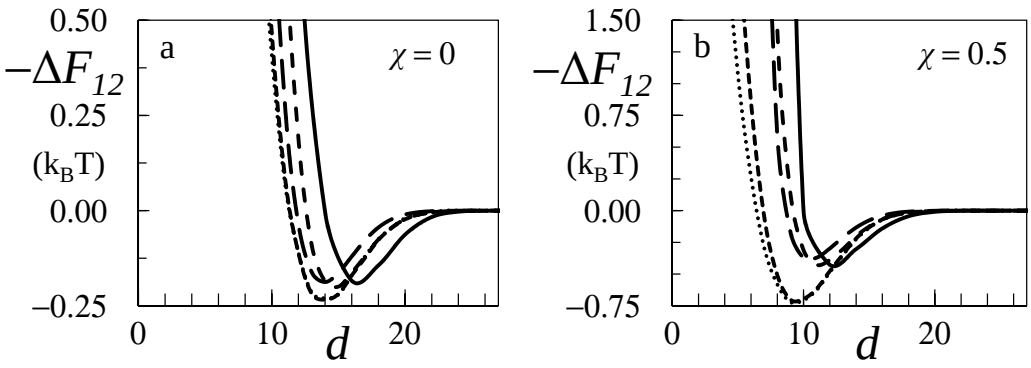

Fig. 12: The effective pair potentials ΔF_{12} in units of k_BT as a function of the distance d in lattice sites, as explained in the text, for $\chi = 0$ (a) and $\chi = 0.5$ (b). The free energies of interactions as presented in fig. 11 have been used for the evaluation of the pair potentials. Again $f = 5$ and $N = 50$. From the dotted line to the continuous line: IP, NoL, cP, FCC and the cell model.

than for the IP. This increase of the distance at which the repulsion occurs could be expected. As the nodes come closer to each other the volume per node becomes smaller until there is not enough space left to fit the polymers. At short distances the interaction potential should thus go to infinity for the cell model, the cP and the FCC configuration. For the NoL and the IP there is still space for the polymers to escape to when the nodes touch each other and the interaction potential grows only modestly.

The well depth for the cell model, cP, and FCC configurations is smaller than for the IP. This is at least partially caused by the delayed onset of the repulsion in the IP. An additional reason is that one node can block bridge conformations between two adjacent nodes reducing the strength of the attraction between those nodes, which is important for bridges made with next nearest neighbours. One would also expect that each additional neighbouring node will decrease the free energy less than the previous one, because fewer chains are remaining for the bridges to form (some are already engaged in bridging). A different way to view this is by considering the entropy due to the number of polymer conformations. With each additional neighbour the number of possible polymer conformations is increased by some amount. Because the free energy scales with the natural logarithm of the number of conformations, the free energy is expected to decrease less with each addi-

tional neighbouring node. The average attraction between the nodes will therefore be lower than for an isolated pair.

The difference between the cell model, cP and FCC configurations is smaller. The depth of the attractive well is almost the same for these three configurations. The curve for the FCC configuration is shifted to a bit smaller distances than that of the cP configuration. This may be because the number of lattice sites that can be reached in a certain number of steps from the node is bigger for the FCC lattice than for a cubic lattice. The volume can thus be used more efficiently with an FCC lattice.

The pair potential obtained from the cell model is thus not such a bad approximation as long as one node is surrounded by many neighbours, that is when the overall node concentration is relatively high. At lower node concentrations, the micelles in the gel will likely form a more porous, open structure wherein each node is no longer surrounded by other nodes on all sides. In this case the cell model will underestimate the attraction and will thus not be able to predict the properties of the gel, such as the critical point for phase separation, correctly.

Based on the interaction free energy given in figure 12 the second virial coefficient, B_2, can be calculated with equation 17. With these B_2 values it is possible to estimate whether the flower-like micelles can phase separate into a dilute and a concentrated gel phase. Vliegenthart et al. reported the critical B_2 values for several forms of the potential. The critical B_2 values ranged from -8.9 to -5.5 times the volume of the repulsive core of the particles.[31] In the same way as Vliegenthart et al., we define a distance d' at which $\Delta F(d) = 0$ for the first time. Based on this distance we calculate the volume of the repulsive core V_{core} of the micelles with equation 18. Subsequently we can calculate a normalised B_{2N} by dividing B_2 by V_{core} as in equation 19.

$$B_2 = \frac{1}{2}\int 4\pi d^2 \left(1 - e^{-\Delta F(d)_{12}}\right) \mathrm{d}d \tag{17}$$

$$V_{core} = \frac{\pi}{6} d'^3 \tag{18}$$

$$B_{2N} = \frac{B_2}{V_{\text{core}}} \tag{19}$$

Using this B_2N we find that for the IP, the boundary for phase separation is the line from $\chi = 0.2$ and $f = 1$ to $\chi = 0.5$ and $f = 10$. For combinations with a lower χ and a larger f the steric repulsion is strong enough to prevent

phase separation. This dependence on the number of polymers per node is opposite to what would be expected and what is found experimentally.[9] As f increases one would expect the number of bridges to increase and thus an increased attraction. This illustrates that the pair potential as found from the IP is not suitable to describe the aggregation of more than two micelles. Alternatively, when the effective pair potential from the cP or FCC configuration is used, no phase coexistence is predicted, even for $\chi = 0.5$ and $f = 10$. These results are also in disagreement with the findings of Filali et. al. who observed phase separation for $f > 6$ for PEO polymers with hydrophobic ends in micelles swollen with oil, although their core was larger relative to the size of the corona.[9] The pair potentials found from the cP or FCC configurations thus under estimate the average attraction between the nodes near the critical point.

The SF-SCF calculations show that the interactions between the nodes are not pairwise additive, clearly exemplified by the large difference between the effective pair potentials of the IP or NoL interaction geometries and the more isotropic interaction geometries. When the pair potentials are used in coarse grained computer simulations, one should take this into account. Especially when the density around the node is not radially isotropic, as expected near a critical point, where fluctuations in density are large, or near an interface between the gel and a dilute solution, artefacts can be expected from having just one pair potential (e.g. tuned for the homogeneous surroundings). Because the attraction is weaker when a node is surrounded by more neighbours, it should be relatively easy to remove some of the neighbouring nodes. The surface tension of such a gel will therefore be relatively low and pores can easily be created. This allows particles and perhaps even other polymer networks to penetrate the gel.

Conclusion

We have performed one- and three-gradient SF-SCF calculations to determine the pair potential between nodes in a network of telechelics for different configurations of the nodes. We used a simple model wherein the two ends of the chain are constrained in predefined nodes and the intermediate segments of the chain are in good or theta solvent.

At small distances between the nodes, the coronas of the flower-like micelles overlap resulting in steric repulsion. At larger distances the increased

entropy due to bridge formation gives attraction. Hence a curve with a local minimum was observed.

With the cell model we found that the position of the minimum scales with the length of the chain N roughly as $N^{\frac{3}{5}}$ and as $f^{\frac{1}{5}}$ with the number of chains per node, as expected from the Daoud-Cotton model.[29] With increasing χ the position of the minimum moved closer to the node and the attraction became 2 to 3 times stronger. The depth of the attractive well also increased with an increasing number of polymers per node. This increase decreased with each additional polymer chain. Roughly scaling as $f^{0.65}$ for $\chi = 0$ and $f^{0.75}$ for $\chi = 0.5$.

For the isolated pair on a simple cubic lattice the same trends were found as for the cell model. Except that the depth of the well scaled with the number of polymers per node as $f^{0.44}$ for $\chi = 0$ and $f^{0.51}$ for $\chi = 0.5$. For both the cell model and the isolated pair there was also a weak trend of decreasing well depth with increasing polymer length at $\chi = 0$.

For the cP and FCC configuration and the cell model, the depth of the attractive well in the effective pair potential was about 60% of that for the isolated pair(IP) and the nodes on a line (NoL) at $\chi = 0.5$. For the FCC and cP configuration the attractive well was shifted outward compared to the IP and NoL configuration, due to the increased steric repulsion. The well of the cell model lies even further out because the volume per node, for a given inter node distance, is the smallest in the cell model and the steric repulsion is thus the strongest. At the same time the attraction has a longer range, as the number of possible end points increases as the cell model becomes bigger. For $\chi = 0$ the depth of the attractive well for the cP and FCC configuration and cell model is about 85% of that of the isolated pair.

In most experimental systems χ is close to 0.5. The strength of the interaction than varies considerably with the number of neighbours the interacting nodes have. This is nicely illustrated when one tries to predict the phase behaviour based on the different pair potentials. Based on the pair potential of the isolated Pair, phase separation should occur over a wide range of f and χ values, whereas based on the potential from the cP or FCC configuration no phase separation will occur within the range of f studied here. Although, following the trend, phase separation is expected to occur at $f \approx 13.5$, which is in turn higher than the experimentally observed critical $f \approx 6$.[9] It is thus important to adjust the interaction potentials based on the average number of neighbours the nodes are expected to have. Ideally one would use a non-pairwise additive potential to calculate these interactions.

Overall the pattern of interaction is the same for the cell model and the other 3D configurations. The interaction however does occur at greater distances for the cell model because the number of nodes seems to increase as the distance between them becomes bigger. The depth of the attractive well is the roughly the same for the cell model and the other densely packed configurations but considerably less deep than that of the isolated pair and chain configurations. Using the cell model to determine the pair interactions for a course grained model will therefore lead to an overestimate of the repulsion at high concentrations and underestimate the attraction at lower concentrations. We can thus conclude that using the potentials of the cell model will underestimate the net attraction between the nodes.

To further study gels with telechelic polymers we are planning to do hybrid Monte Carlo SF-SCF simulations, in which the nodes are moved by a Monte Carlo scheme and the SCF equations are solved for each snapshot. In such a simulation the pair potential does not need to be imposed as in particle based MC simulations. A preliminary paper, showing the feasibility of this approach, has recently been published[32].

Another avenue of future research is the study of micelles made of ABC polymers, similarly to the micelles made of ABA polymers. As all the polymers need to form bridges it is expected that the two types of ABC micelles will attract each other much stronger than ABA micelles. Such networks would be stiffer and stronger than ABA networks while retaining their self healing properties.

Acknowledgements

This research was funded by NWO, The Netherlands Organization For Scientific Research.

References

[1] J. François, S. Maitre, M. Rawiso, D. Sarazin, G. Beinert, and F. Isel. Neutron and x-ray scattering studies of model hydrophobically end-capped poly(ethylene oxide) aqueous solutions at rest and under shear. *Colloids and Surfaces A: Physicochemical and Engineering Aspects*, 112:251–265, 1996.

[2] X.-X. Meng and W. B. Russel. Rheology of telechelic associative polymers in aqueous solutions. *J. Rheol.*, 50:189–205, 2006.

[3] Atsushi Harada and Kazunori Kataoka. Formation of polyion complex micelles in an aqueous milieu from a pair of oppositely-charged block copolymers with poly(ethy1ene glycol) segments. *Macromolecules*, 28:5294–5299, 1995.

[4] M. Lemmers, J. Sprakel, I. K. Voets, J. van der Gucht, and M. A. Cohen Stuart. Multiresponsive reversible gels based on charge driven assembly. *Angewandte Chemie*, 122:720–723, 2010.

[5] J. Wang, M. A. Cohen Stuart, A. T. M. Marcelis, M. Colomb-Delsuc, S. Otto, and J.van der Gucht. Stable polymer micelles formed by metal coordination. *Macromolecules*, 45:7179–7185, 2012.

[6] A. N. Semenov, J.-F. Joanny, and A. R. Khokhlov. Associating polymers: Equilibrium and linear viscoelasticity. *Macromolecules*, 28:1066–1075, 1995.

[7] J. Sprakel, N. A. M. Besseling, M. A. Cohen Stuart, and F. A. M. Leermakers. Phase behavior of flowerlike micelles in a SCF cell model. *The European Physical Journal E*, 25:163–173, 2008.

[8] E. Michel, J. Appell, F. Molino, J. Kieffer, and G. Porte. Unstable flow and non-monotonic flow curves of transient networks. *J. Rheol.*, 45:1465–1477, 2001.

[9] M. Filali, R. Aznar, M. Svenson, G. Porte, and J. Appell. Swollen micelles plus hydrophobically modified hydrosoluble polymers in aqueous. *J. Phys. Chem. B*, 103:7293–7301, 1999.

[10] T. Liu, D. Liang, L. Song, V. M. Nace, and B. Chu. Spatial open-network formed by mixed triblock copolymers as a new medium for double-stranded dna separation by capillary electrophoresis. *Electrophoresis*, 22:449–458, 2001.

[11] A. J. de Graaf, I. I. Azevedo Próspero dos Santos, E. H. E. Pieters, D. T. S. Rijkers, C. F. van Nostrum, T. Vermonden, R. J. Kok, W. E. Hennink, and E. Mastrobattista. A micelle-shedding thermosensitive hydrogel as sustained release formulation. *Journal of Controlled Release*, 162:582–590, 2012.

[12] D. C. Tuncaboylu, M. Sari, W. Oppermann, and O. Okay. Tough and self-healing hydrogels formed via hydrophobic interactions. *Macromolecules*, 44:4997–5005, 2011.

[13] J.-F. Berret and Y. Séréro. Evidence of shear-induced fluid fracture in telechelic polymer networks. *Physical Review Letters*, 87(048303), 2001.

[14] J. Sprakel, E. Spruijt, J. van der Gucht, J. T. Padding, and W. J. Briels. Failure-mode transition in transient polymer networks with particle-based simulations. *Soft Matter*, 5:4748–4756, 2009.

[15] J. M. H. M. Scheutjens and G. J. Fleer. Statistical theory of the adsorption of interacting chain molecules. 1. partition function, segment density distribution, and adsorption isotherms. *The Journal of Physical Chemistry*, 83:1619, 1979.

[16] G. J. Fleer, M. A. Cohen Stuart, J. M. H. M. Scheutjens, T. Cosgrove, and B. Vincent. *Polymers at Interfaces*. Chapman & Hall, London, 1993.

[17] O. A. Evers, J. M. H. M. Scheutjens, and G. J. Fleer. Statistical thermodynamics of block copolymer adsorption. 1. formulation of the model and results for the adsorbed layer structure. *Macromolecules*, 23(5221-5232), 1990.

[18] J. M. H. M. Scheutjens and G. J. Fleer. Statistical theory of the adsorption of interacting chain molecules. 2. train, loop, and tail size distribution. *J. Phys. Chem.*, 84:178, 1980.

[19] J. M. H. M. Scheutjens and G. J. Fleer. Interaction between two adsorbed polymer layers. *Macromolecules*, 18:1882–1900, 1985.

[20] S. P. F. M. Roefs, J. M. H. M. Scheutjens, and F. A. M. Leermakers. Adsorption theory for polydisperse polymers. *Macromolecules*, 27:4810–4816, 1994.

[21] M. Charlaganov and F. A. M. Leermakers. Molecular modeling of intermolecular and intramolecular excluded volume interactions for polymers at interfaces. *J. Chem. Phys.*, 131:244115, 2009.

[22] B. R. Postmus, F. A. M. Leermakers, and M. A. Cohen Stuart. Self-consistent field modeling of adsorption from polymer/surfactant mixtures. *Langmuir*, 24:6712–6720, 2008.

[23] F. A. M. Leermakers, J. M. H. M. Scheutjens, and J. Lyklema. On the statistical thermodynamics of membrane formation. *Biophysical Chemistry*, 18:353–360, 1983.

[24] M. Charlaganov, O. V. Borisov, and F. A. M. Leermakers. Modeling of triblock terpolymer micelles with a segregated corona. *Macromolecules*, 41:3668–3677, 2008.

[25] C. M. WijmansJ F. A. M. Leermakers and G. J. Fleer. On the structure of polymeric micelles: Self-consistent-field theory and universal properties for volume fraction profiles. *Macromolecules*, 28:3434–3443, 1995.

[26] P. J. Flory. Thermodynamics of high polymer solutions. *J. Chem. Phys.*, 10:51–61, 1942.

[27] Alexander D. MacKerell Jr. y Hwankyu Lee, Richard M. Venable and Richard W. Pastor. Molecular dynamics studies of polyethylene oxide and polyethylene. *Biophysical Journal*, 95:1590–1599, 2008.

[28] D. C. Liu and J. Nocedal. On the limited memory bfgs method for large scale optimization. *Mathematical Programming*, 45:503–528, 1989.

[29] M. Daoud and J. P. Cotton. Star shaped polymers : a model for the conformation and its concentration dependence. *J. Physique*, 43:531–538, 1982.

[30] C. M. Wijmans and E. B. Zhulina. Polymer brushes at curved surfaces. *Macromolecules*, 26:7214–7224, 1993.

[31] G. A. Vliegenthart and H. N. W. Lekkerkerker. Predicting the gas-liquid critical point from the second virial coefficient. *Journal of Chemical Physics*, 112:5364–5369, 2000.

[32] F. A. M. Leermakers, J. Bergsma, and J. van der Gucht. Hybrid monte carlo self-consistent field approach to model a thin layer of a polyelectrolyte gel near an adsorbing surface. *The Journal of Physical Chemistry A*, 116:6574–6581, 2012.